JOURNAL OF THE ROYAL SOCIETY Interface

The smaller your mouth, the longer your snout: predicting the snout length of *Syngnathus acus*, *Centriscus scutatus* and other pipette feeders

Marc H.E de Lussanet and M Muller

J. R. Soc. Interface 2007 **4**, 561-573
doi: 10.1098/rsif.2006.0201

JOURNAL OF THE ROYAL SOCIETY Interface

J. R. Soc. Interface (2007) **4**, 561–573
doi:10.1098/rsif.2006.0201
Published online 23 January 2007

The smaller your mouth, the longer your snout: predicting the snout length of *Syngnathus acus*, *Centriscus scutatus* and other pipette feeders

Marc H. E. de Lussanet[1,*] and M. Muller[2]

[1]*Psychologisches Institut II, Münster University, Fliednerstrasse 21, 48149 Münster, Germany*
[2]*Experimental Zoology Group, Department of Animal Sciences, Wageningen University and Research Centre, Marijkeweg 40, 6709 PG Wageningen, The Netherlands*

Like most ray-finned fishes (*Actinopterygii*), pipefishes (*Syngnathoidei*) feed by suction. Most pipefishes reach their prey by a rapid dorso-rotation of the head. In the present study, we analysed the feeding kinematics of the razor fish, *Centriscus scutatus*, and of the greater pipefish, *Syngnathus acus* in detail. We found capture times of as little as 4–6 ms for *C. scutatus* and 6–8 ms for *S. acus*. We then hypothesized that the long snout of pipefishes is optimal for such fast feeding. To test this, we implemented in a mathematical model the following considerations. To reach the prey as fast as possible, a low moment of inertia increases the head's angular speed, whereas a long snout decreases the angle over which the head must be turned. The model accurately predicted the snout lengths of a number of pipefishes. We found that the optimal snout length, with which a prey will be reached fastest, is inversely related to its cross-section. In spite of the small cross-section, the development of a long snout can be an evolutionary advantage because this reduces the time to approach the prey.

Keywords: prey capture; feeding mechanism; dynamic model; pipefish; biomechanics

1. INTRODUCTION

Ray-finned fishes (*Actinopterygii*) are the largest and most diverse group of living fishes (Nelson 1984). Most of them feed by suction and approach the prey by swimming and by jaw protrusion (Kayser 1961; Alexander 1967*a*,*b*; Motta 1984; Van Leeuwen & Muller 1984; Muller 1996). Jaw protrusion is energetically very efficient and is very fast (Osse 1985), but is generally short ranged. Swimming is suitable to bridge longer distances, but it takes longer to accelerate the whole body than just the mouth (Van Leeuwen 1984).

Another technique to capture prey is by a dorso-rotation (lifting) of the head, including the entire mouth (Alexander 1969, 1970; Osse 1969; Muller & Osse 1984; Muller 1987). This technique has been described in the light of the suction mechanism and is known as 'pipette feeding' (Alexander 1969, 1970; Lauder 1980; Muller 1987), although we prefer to call it '*pivot feeding*' as will become clear in this manuscript. Accelerating just the head, not the entire body, is potentially very effective to rapidly approach the prey. This may be so for typical pivot feeders such as pipefishes, but also for short-snouted fishes of different shapes. For example, in studied prey catches by the flatfish *Platichthys flesus*, head rotation translated the mouth by about as much as the whole-body movement did (Muller & Osse 1984). In addition, judging from the skull mechanism, *Chauliodus sloani* may rotate its cranium by 90° before taking in a prey (Tchernavin 1953; Muller 1987). Even though *Chauliodus* has no elongated head, such a large rotation may give a considerable contribution to the catching of prey. Therefore, possibly, the pipefishes represent just one extreme on a wide range of pivot feeders.

The suborder of *Syngnathoidei* (order: *Gasterosteiformes*; see Nelson 2006) contains some of the most exotic and attractive members of bony fishes, among them are the pipefishes, pygmy seahorses and seahorses (*Syngnathidae*), razorfishes (*Centriscidae*) and snipefishes (*Macrorhamphosidae*) (Jungersen 1910; Altermatt 1991; Kuiter 2000). For simplicity, we will call members of these families 'pipefishes' throughout the present study. Some pipefishes are among the fastest feeding vertebrates known (cf. Deban & Olson 2002), with 7.5 ms for the syngnathid *Entelurus aequoreus* (Muller & Osse 1984) and 5.5 ms for the seahorse *Hippocampus erectus* (Bergert & Wainwright 1997). The three mentioned families of pipefishes (and presumably also the ghostfishes, *Solenostomidae*) are specialized in a dorso-rotation

*Author for correspondence (lussanet@psy.uni-muenster.de).

Electronic supplementary material is available at http://dx.doi.org/10.1098/rsif.2006.0201 or via http://www.journals.royalsoc.ac.uk.

Received 31 October 2006
Accepted 27 November 2006

of the head to approach a prey. Most of them possess a long snout with a small, upward-facing mouth at the end. Many of them feed from an almost stationary position.

Although detailed anatomical descriptions exist for a number of syngnathoid fishes (Jungersen 1908, 1910; Branch 1966; Altermatt 1991), kinematic data of the feeding act are sparse (Muller & Osse 1984; Muller 1987, 1996; Bergert & Wainwright 1997). A detailed kinematic analysis has not been published yet for any pipefish species.

In the present study, we hypothesize that a long snout is an adaptation to reach a prey as fast as possible through a head rotation (which we name pivot feeding). With a model, we will analyse the conditions for which a long snout is optimal for fast feeding. We will verify the model with experimental data. We will first present a detailed analysis of the feeding kinematics in two species from different families, *Syngnathus acus* (greater pipefish) and *Centriscus scutatus* (razorfish). On the basis of this analysis, we formulate the model. With this model, we will then compare the measured and the predicted optimal snout length for 34 specimens of about 17 species of pipefishes. We will discuss the model predictions and the general relevance for using a rapid head turn to capture prey.

The relatively stationary body position makes pipefishes well suited for testing our hypothesis. Moreover, the head is highly rigid in the plane of rotation. In *Syngnathidae*, the anterior vertebrae are stiffened and even fused (Jungersen 1908, 1910; Branch 1966). The rapid head rotation is driven by the epaxial musculature, either through direct contraction or indirectly, by elastic energy stored in the tendons that insert on the cranium, or both (Muller 1987). A four-bar linkage locks the head in a depressed position. Release of this locking mechanism triggers the head's launch towards the prey (Branch 1966; Muller 1987, 1996; Aerts 1991). *Syngnathidae*, such as the greater pipefish *S. acus*, slowly orient towards a prey before catching it in a stroke. The razor fish *C. scutatus* can adopt any orientation (preferentially head-down) while making up to 5–10 prey capture movements per minute. It is laterally strongly flattened (Jungersen 1908; Altermatt 1991).

2. METHODS

In this section, we describe how we recorded high-speed movies of *S. acus* and *C. scutatus* in simultaneous lateral and ventral views. From these movies, we analysed in detail the kinematics of the centre of rotation, head volume, and head and body orientations. These data served as a basis for the model. Where possible, we measured the movements of the lower jaw and the hyoids. In order to validate the model, we collected morphological data of a number of preserved specimens of approximately 17 species of pipefishes (the nominal status of some specimen was uncertain, see appendix B).

2.1. High-speed movie recording

All fishes were trained to feed under the experimental conditions. They were trained until they made the same number of feedings under the experimental light conditions as under normal light conditions. The adult *S. acus* were fed mysid shrimp (*Neomysis* sp.), which were mounted to fix the feeding location. The *C. scutatus* and the juvenile *S. acus* were fed with free-swimming 2-day-old *Artemia salina* nauplii larvae. Specimen of *S. acus* came from Waddenzee; *C. scutatus* were provided by a local reseller.

In order to get the highest possible spatial and temporal accuracy and resolution, we selected the films on the following criteria. The camera must have reached a filming speed of at least 1000 frames per second, the yaw and roll angles must be smaller than 20° and the head must be focused. In total, five movies out of a large number of feeding movements made by several specimens fulfilled these criteria. Apart from this, the selected feeding movements were in no way exceptional with respect to the other recorded captures, as far as we could judge. Out of these five, three were by a single *C. scutatus*, and two by a single *S. acus*.[1]

The high-speed movies were made with a 55 mm objective using 16 mm film (25 DIN, Double-X Negative; camera: John Hadland Ltd, UK). The exposure time was 0.2 ms and a diaphragm of 5.6–8.0 was used. The exact inter-frame intervals were interpolated from 250 Hz spots on one edge of the film. Twenty 1000 W halogen lights provided enough illumination to produce a good image on the film. A 45° backward-tilted mirror placed below the fish provided a ventral view to the camera's side view, in the same image.

A juvenile *S. acus* (16-day post-hatching, head length 3.5 mm) was shadow filmed with an exposure time of 0.4 ms, with an 80–200 mm zoom lens (Nikon), diaphragm 11. In the shadow film technique, a single light source is placed behind the fish, so that only its contour is recorded. For this, the light of a 50 W halogen illumination (Philips 12336H3) was bundled using a lens, before passing through the fish tank towards the camera. Again, a ventral view was simultaneously recorded via tilted mirror, which reflected a single light source from above the fish (Drost & van den Boogaart 1986). Unfortunately, the selection criteria given above were not fulfilled in any of the films of the juvenile *S. acus*, so we selected the best one (figure 1*e*). In this movie, the roll angle was 40° and the yaw angle 35°.

2.2. Analysis of the movies

Time $t=0$ was defined as the last movie frame before the start of the fast movement phase. Each movie frame was back-projected on transparent paper and manually traced twice. Apart from tracing the contours, we selected anatomical landmarks on the body, head and aquarium, which were non-deforming and were continuously visible. A scale bar, mounted to the aquarium, was traced as well. From the selected landmarks, the rotations and centres of rotation of the skull and the body with respect to the aquarium

[1]The method we used is highly accurate, both spatially and temporally. However, an important disadvantage of using a conventional camera instead of modern CCD and digital filming techniques is that the collection of data is laborious. As a film lasts only about 15 s at high speed filming, the camera needs time to accelerate, and the fishes feed at unpredictable instants.

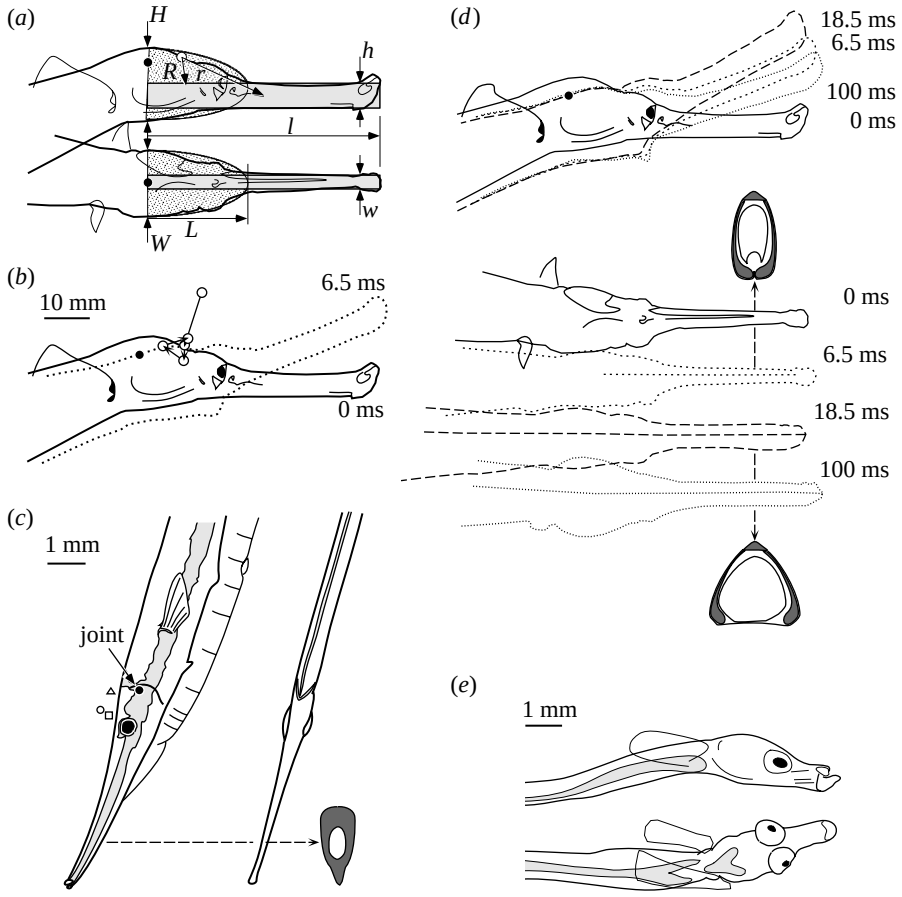

Figure 1. (*a*) Fitted volumes to estimate the moments of inertia. (*b*) Tracings of capture 2 of *S. acus* (squares in figure 2*f*): the last frame before the hyoid started to move (t=0 ms) and the last frame before the prey was captured (t=6.5 ms, dotted). The dot marks the location of the neck joint. The circles mark the centres of rotation between frames 1–3 (top one) and between the following subsequent frames. (*c*) *C. scutatus*. The open circles mark the centre of rotation shown for the three sequences in figure 2*b*. The centre of rotation was constructed between the first tracings of hyoid depression and the last tracings before prey capture. The inset shows the enlarged cross-section through the snout. (*d*) Lateral and ventral tracings from capture 2 of *S. acus*. Note the depression of the body during the fast phase. For clarity, the ventral traces were not printed on top of each other. Note the compression and expansion of the head and the snout, also shown as enlarged cross-sections. (*e*) Tracing of the first frame of the juvenile *S. acus*.

were reconstructed in both the ventral and lateral views. To find a centre of rotation, we mounted a small piece of millimetre paper to one tracing, in the vicinity of the centre of rotation. We then aligned reference landmarks of the second tracing with the first one and marked the millimetre grid on the second one. The centre of rotation was then accurately found after aligning the target landmarks.

The yaw angle and the projected pitch angle of the head and the body were measured from the tracings. From these, the true pitch angle was calculated. The roll angle was calculated as the tilt of the plane in which the head rotated. From these angles, we calculated the *neck angle* between head and body (0° is defined as the minimal neck angle measured in the analysed movies), and the *lift angle* of the head with respect to t=0, in the Earth-bound frame of reference. The locations of the hyoid joints were measured from an X-ray of the fish. The depression angle of the hyoid with respect to t=0 was measured from the hyoid tip in the tracing. From each tracing, we also measured the maximal distance between the opercula and the width and the height of the snout.

Unfortunately, in the movies of *S. acus*, there were no suitable landmarks on the body to determine its exact caudo-rostral translation. As a result, in *S. acus*, the head's lift angle was much more reliable than the neck angle.

To determine the accuracy of these measurements, we performed the complete procedure twice, once using the first tracings of each movie and the next time using the second tracings of the same movies. The standard deviations of the differences between these two independent analyses are shown as error bars in the figures.

2.3. Stereo photographs and moment of inertia

The 34 preserved specimens (appendix B) were stereo X-ray photographed for measurements (lateral and dorsal views). Snout length was measured from the neck joint,[2] with the mouth closed (figure 1*a*). Snout width and height were measured at the joint of the mandibula (lower jaw) on the quadrate, in mouth-closed and maximally adducted positions. The head

[2]The model assumes that the snout continues within the head base (figure 1*a*). We also made the simulations without this assumption to check that this error is very small, and falls well within the accuracy range of the estimated head volume. We therefore chose for this simplification.

height was measured as the minimal diameter through the neck joint. The head width was measured between the opercula, and head length was defined as the distance from the centre of the neck joint to the caudal point where the mesethmoid and the parasphenoid meet.

The head volume without the snout was approximated as a half-ellipsoid with its base through the neck joint and a maximal cross-section of head height × head width. The snout volume was approximated as a tube with an elliptical cross-section (the volumes and the moments of inertia for such shapes can be found in textbooks of physics). As measured from the movie tracings (figure 1*b*,*c*), the centre of rotation in *C. scutatus* and *S. acus* was just above the cranium, halfway between the eye and the neck joint. We assumed that this was the centre of rotation in all species of appendix B. The moments of inertia were calculated with respect to this hypothetical centre of rotation of the head:

$$J_{\text{head}} = \alpha\frac{\rho\pi WHL}{6}\left(\left(\frac{1}{5}-\frac{9}{64}\right)L^2+\frac{H^2}{20}+R^2\right)$$

$$J_{\text{snout}} = \alpha\frac{\rho\pi whl}{4}\left(\frac{l^2}{12}+\frac{h^2}{16}+r^2\right)\quad(\text{kg m}^2) \qquad (2.1)$$

where the parameters outside the parentheses are the mass, and the parameters inside are the moment of inertia factor with respect to the centre of mass plus the quadratic distance (r^2, R^2) to the centre of rotation (Steiner's theorem). The mass is the volume multiplied with ρ (the average density of the tissues and water inside the cavities). An object that accelerates in water will also accelerate surrounding water, which effectively increases the object's mass. Daniel (1984) gives the added mass coefficients for elliptic cylinders of different aspect ratios. On the basis of these coefficients, we estimated correction factors for the effective mass as $\alpha = 1.5$ for *C. scutatus*. For *S. acus* we estimated $\alpha = 1.5$ for the snout and $\alpha = 2.0$ for the head segment. The measures w, h, l, r, W, H, L, and R are shown in figure 1*a* and appendix C, and are provided as electronic supplementary material.

3. RESULTS

We first describe the feeding kinematics of the species *S. acus* and *C. scutatus*. On the basis of these measurements, we will then derive the model. With this model, we predict the optimal snout lengths and the relation between optimal snout length and snout diameter (prey size), and we will compare these data with the measurements of preserved specimens.

3.1. *Feeding kinematics in* C. scutatus

In the razorfish, *C. scutatus*, each capture started with a (relatively slow) depression of the head from a 3° resting neck angle to a neck angle of 0–0.6°, in approximately 25 ms (figure 2*a*). At the end of the fast phase, after the prey was caught, the head reached its maximal excursion around $t = 10$ ms. From this maximum excursion, the head swung back to its resting elevation of approximately 3° neck angle. This resting angle was reached after approximately 100 ms. In the aquarium, the fishes typically made capture movements at a rate of 6–10 min^{-1}. The next capture movement could start a few seconds after the end of the previous one.

Figure 2*b* shows the fast phase. The *C. scutatus* caught the prey within 6 ms and once even within 5 ms (figure 2*b*, capture 2). The regression lines in panel 2*c* demonstrate that a constant acceleration badly describes the head rotation. Rather, the head accelerated for not more than a single movie frame (0.7 ms) before reaching an almost constant angular velocity of 35 rad s^{-1} (figure 2*b*). The average angular acceleration in the first frame was 50×10^3 rad s^{-2}. The angular velocity remained constant for 3–4 ms, after which the mouth opened and the head decelerated. The mouth remained closed for most of the lifting movement, at least in the two movies where the time of opening could be observed with certainty. Therefore, for most of the head's lifting phase, no externally sucked water flowed through the snout. This is remarkable: the feeding canal through the snout is a rigid tube, but the buccal volume was increased by the increasing neck angle. This volume increase can only have been compensated by adduction of the opercula. We could not observe these opercular movements from the films due to the (small) roll angles in the movies.

As an additional check for the accuracy of the measured angles, we plotted the measured relation between neck angle and hyoid depression angle (figure 2*d*). This relation indeed was close to that predicted from the linkage which is formed by the urohyal–pelvic girdle–cranium–hyoid (Muller 1987). The angle over which the head turned differed by as much as 1.9° between captures 9 and 10 (figure 2*b*). This variability seems to reflect a remarkable flexibility in the execution of the movement, considering that the goal was reached within just 5.5 ms. In all the three feeding movements, the body made a counter rotation of 1.0° until the time of prey capture.

3.2. *Feeding kinematics in* S. acus

Figure 2*e* shows the captures by *S. acus*. It shows the spatial head lift angle rather than the neck angle because the body orientation could not be determined as reliably and accurately as the head orientation. *S. acus* typically fed at a rate of 0.5–2 min^{-1}, much lower than *C. scutatus*. A prey capture sequence always began with a gradual head depression during which the animal positioned its mouth to the prey. Differently than in *C. scutatus*, the fast phase started after a clear stationary period of variable duration (greater than 100 ms). Remarkably, the first peak in the lift angle at the end of the fast phase was not the maximal excursion. The maximal excursion was reached later, at $t = 25$–50 ms. We observed this double peak in the lift angle in many movies.

As in *C. scutatus*, the fast phase started with hyoid depression (figure 2*f*). However, in *S. acus*, the angular acceleration remained almost constant until the prey was swallowed (figure 2*g*). The high regression coefficients ($R^2 > 0.99$) indicate that the accelerations were indeed

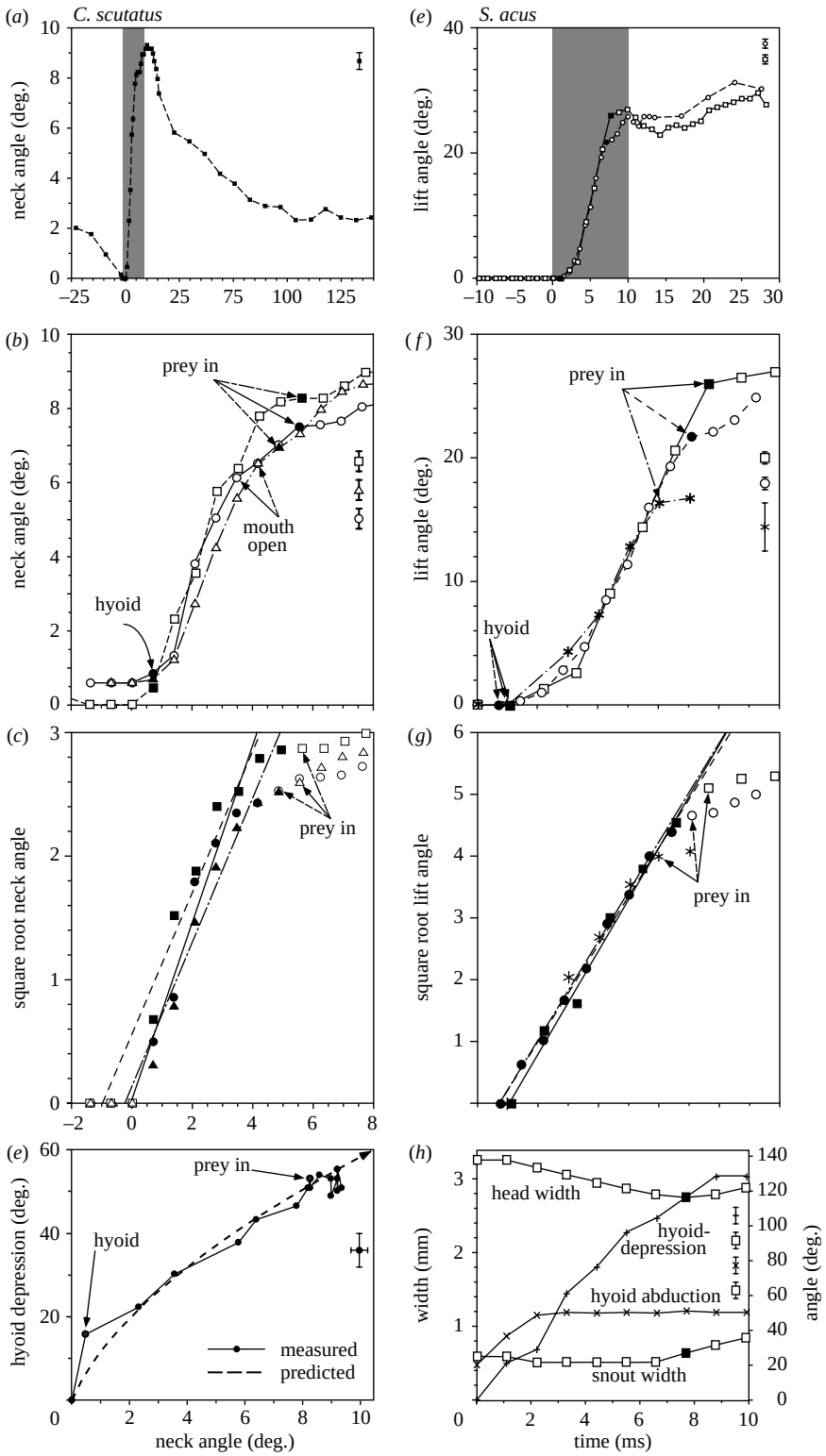

Figure 2. Feeding kinematics from high-speed movies for *C. scutatus* (*a–d*) and *S. acus* (*e–h*). (*a*) Neck angle in *C. scutatus*, capture 2. (*b*) A shorter time window (shaded grey in *a*) and two additional actions by the same specimen. At the time of capture, the body counter rotation was 1.0° in each sequence. Circles and continuous line: capture 1, squares and dashed line: capture 2, triangles and dash-dotted line: capture 3. (*c*) The square root of the neck angles of (*b*). The regression lines are fitted to the filled symbols ($R^2 = 0.87$–0.90). (*d*) Measured (continuous) and predicted (dashed) relation between hyoid rotation and neck angle for capture 2. (*e*) Head lift angle in *S. acus*. The two prey capture actions were by the same adult. (*f*) A shorter time window of the same sessions (shaded grey in *e*). The body counter rotation at 7 ms was 4.8° in both. Asterisks: 16-day juvenile *S. acus*. (*g*) The square root of the lift angles in (*f*). Slope of linear regression lines (fit on the filled symbols): 0.78 $\mathrm{deg}^{0.5}\,\mathrm{ms}^{-1}$ (circles); 0.84 $\mathrm{deg}^{0.5}\,\mathrm{ms}^{-1}$ (squares); 0.83 $\mathrm{deg}^{0.5}\,\mathrm{ms}^{-1}$ (juvenile); $R^2 > 0.99$. (*h*) During the head's acceleration, the snout width was constant until the mouth opened, whereas the distance between the opercula decreased. All angles are corrected for three-dimensional orientation and projection. Error bars show the standard deviation of the differences between two analyses of the same movie (see §2). $t = 0$ is the last frame before the hyoid appears in the side view. For the captures where this was observable, the frame where the prey was ingested is marked by a symbol of inverted filling.

constant. The regression slopes of 0.8 $deg^{0.5}$ ms^{-2} imply that these accelerations were around 22×10^3 rad s^{-2}. In the presented feeding movements, the time of mouth opening was not detectable, but from other movies of adult *S. acus*, we observed that the mouth never opened more than a single movie frame (0.7–1.5 ms) before prey capture. Although the acceleration profile was very similar in the two measurements, the neck angle at which the prey was caught differed by 4°. After the prey was caught, the head abruptly decelerated and reached its maximal excursion at a much slower rate (figure 2*e*). For both *S. acus* and *C. scutatus*, the head's centre of rotation was located caudo-dorsally from the eyes (figure 1*b*,*c*). Even the juvenile *S. acus* showed a very similar movement. The prey was caught slightly faster and at a lower lift angle. Note, however, that the measurement of the juvenile was much less reliable than that of the adult specimen.

Figure 1*d* shows four traced frames of capture 2. The length and the orientation are corrected for yaw and roll. During the fast phase, the anterior part of the body moved down, pushing the head forward. The width of snout and head changed at different instances (ventral view of figure 1*d*,*h*). The snout's width was constant and minimal until the last frame before the prey was caught. One frame later, the prey was already sucked in. The snout then expanded, reaching its maximum width around 18 ms. The head's maximal width (i.e. between the buccal plates) gradually decreased until 6.5 ms. It then gradually abducted again, reaching its greatest width at $t=100$ ms (figure 1*d*).

Figure 2*h* shows the abduction movements for the fast phase of capture 2. It shows that the abduction sequences of the opercula, hyoids and snout were very different, even in the fast phase. The fast phase started with hyoid abduction within the first 2 ms, and coincided with the depression–retraction movements of the hyoid, which lasted for the entire fast phase.[3] The snout width decreased during the first frames of the fast phase and started increasing as soon as the mouth opened. The opercula became more adducted throughout the fast phase. The coincidence of hyoid abduction and snout adduction reflects the mechanical flexibility of the suspensory structures.

3.3. *Hyoid morphology in* S. acus *and* C. scutatus

Figure 3 shows schematically the mechanism of the hyoid, as part of the urohyal–pelvic girdle–cranio-suspensory linkage (Muller 1987), and the main muscles involved. This system is essential for a proper understanding of the feeding mechanism of *Syngnathidae* but was not included in earlier descriptions (Jungersen 1910; Branch 1966), so we give a brief description here. In *S. acus*, cranial pitch movements are driven by the epaxial musculature and its antagonists, the hypaxial musculature and the *m. sterno-hyoideus*. The epaxial and hypaxial musculature do not connect with the pectoral girdle or the anterior vertebrae, but run through small foramina and insert on the urohyal. The *m. cranio-cleithrales* do exert a small depressing moment, but a large lateral moment on the skull, and are presumably responsible for the flexible lateral movements of the head (approx. 20° yaw to each side). Not shown is the *m. pharyngo-cleithralis*, which inserts on the base of the hyoid, and connects the ventral base of the gill arches. The interhyal forms a ball joint of the hyoid arch with the *hyomandibula* (Anker 1989), enabling depression as well as rotation about the long axis of the hyoid (Jungersen 1910). The paired hyoids together form a hinge joint (figure 3*b*; Aerts 1991). We measured in *S. acus* an angle of 40–90° between the hyoids in the plane through the three joints, as shown in the figure. Abduction of the hyoids is linked with abduction of the *hyomandibula* and is driven by retraction of the urohyal (Aerts 1991). In *S. acus*, the antagonist is the *m. add. arcus palatini* (figure 3*a*). In an adducted and folded position, the ceratohyal forms a rim, which fits into grooves of the hyomandible (Jungersen 1910). In dead specimens, we found that hyoid depression is possible only after some abduction, for which the relaxation of *m. add arc. pal.* is necessary.

The functional morphology in *C. scutatus* is very different from *S. acus*. In *C. scutatus*, the feeding canal of the snout cannot be abducted (figure 1*c*). The hyoids are tightly connected narrow and relatively short. Therefore, there is virtually no abduction of the hyoids (cf. figure 2*h*). The hypaxial musculature inserts on the pectoral girdle and has no direct connection to the urohyal.

3.4. *Discussion of the feeding mechanism*

The prey capture times of 4–6 ms for *C. scutatus* are among the shortest ever reported for vertebrates. The 6–8 ms for *S. acus* are similar to those reported for *E. aequoreus* (Muller & Osse 1984) and *H. erectus* (Bergert & Wainwright 1997). These times also fall in the range that we observed in the many movies of a number of specimens that we made. As *S. acus* under natural conditions also slowly positions itself before catching a relatively stationary prey, the mounting of the food is unlikely to have influenced the feeding movement. However, we observed that *S. acus* can rotate its head even faster when it is not catching a prey. We filmed how *S. acus* repetitively hit a shrimp with its snout while turning the head about twice as fast as in the suction feeding sessions that we present here. With this feeding technique, the shrimp was cut into pieces small enough to swallow.

Immediately following the prey capture, the head decelerated briefly (figure 2*b*,*f*). This deceleration was most pronounced in *S. acus*. As this deceleration immediately follows on the opening of the mouth, it seems plausible that some kinetic energy of the head movement is transformed in the forceful suction needed to catch the prey.

The feeding mechanism of *C. scutatus* and *S. acus* is highly specialized. The specific findings for *S. acus* can probably be extended to most *Syngnathidae* (possibly except *Hippocampus*), but not to other gasterosteiform

[3]We did not plot the relation between hyoid movement and neck angle, because the hyoid bar becomes shorter in the lateral projection and the 'urohyal'-bar decreases due to muscle contraction (Muller 1987).

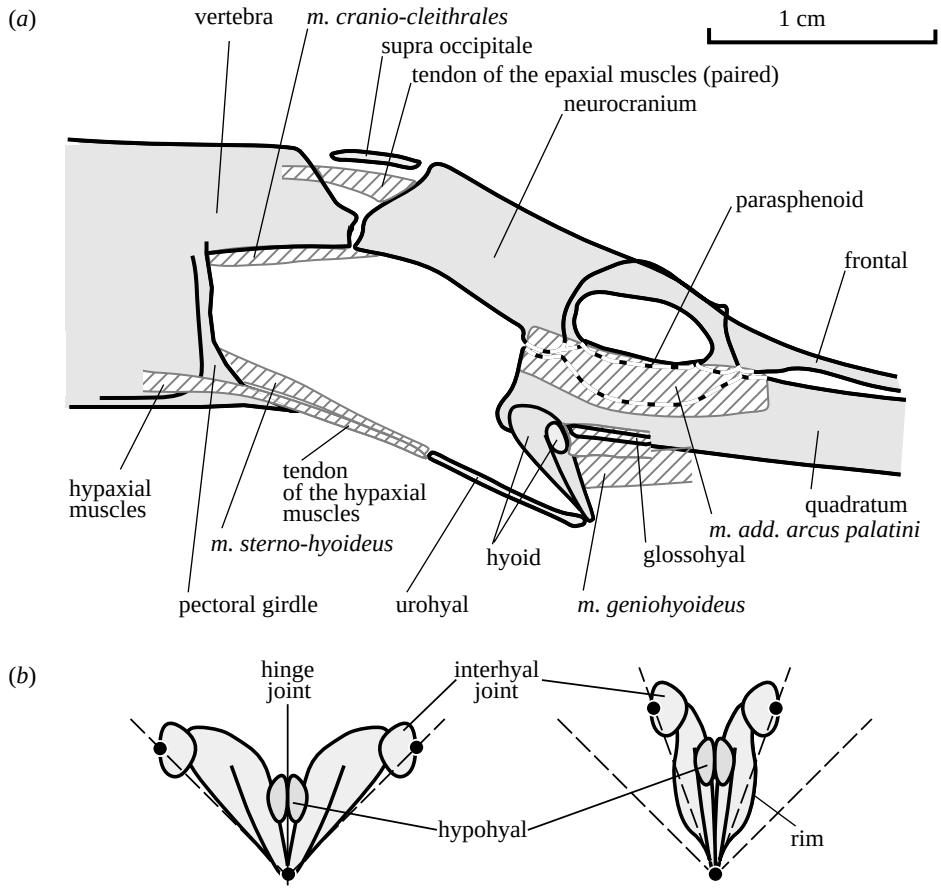

Figure 3. Schematic medial view of the dissected buccal space of *S. acus*, after removal of the gill arches and the *m. pharyngo-cleithralis*. (*a*) The major muscles for controlling the head movements in feeding. (*b*) Schematic ventral view on the hyoids in maximally abducted and adducted positions. Each hyoid has a joint on the *hyomandibula*, as well as two joints on the other hyoid, such that the hyoids form a hinge joint (cf. Aerts 1991).

families. For example, *Macrorhamphosus scolopax* has quite different specialized features of the feeding apparatus which partly resemble *C. scutatus* and partly *S. acus* (Altermatt 1991). Moreover, we found a number of remarkable differences between *C. scutatus* and *S. acus*.

Firstly, the snout of *S. acus* can laterally greatly expand, whereas that of *C. scutatus* is rigid. During the fast phase, the snout of *S. acus* is therefore much narrower than the prey that fits through it, which decreases the moment of inertia, and which could have implications for the optimal snout length (see §4).

Secondly, the hyoid mechanism is quite different in these two species. During the fast phase of feeding, the hyoid abduction in *S. acus* is not related to suction, since it is not linked with opercular or snout abduction and occurred when the mouth was closed. Our findings suggest that hyoid abduction could trigger hyoid depression. What speaks for this is that the rim of the adducted hyoid fits into the suspensory, and that the abduction appears to be linked to the depression of the hyoid (figure 2*h*). This is different to the mechanism in *Haplochromis elegans* (Aerts 1991), where the hyoid abduction occurs when depression is almost completed. Thirdly, in *C. scutatus*, the fast head lifting phase was immediately preceded by a fast head depression, whereas in *S. acus*, the fast lifting phase started from a stationary period. This difference could also be related to the trigger mechanism, for example, it is possible that the head depression at some point makes the locking mechanism unstable as suggested by Muller & Osse (1984). In our view, the complex issue of the triggering cannot be regarded as solved yet.

Finally, the velocity profile of the head rotation in the fast phase differed strongly. This could indicate that different mechanisms power the fast phase. We consider two idealized cases: one based on elastic tendon energy and another based on active muscle contraction. An elastic tendon can store a specific amount of elastic energy which is converted to kinetic energy. This mechanism will give the shortest reach time if all this kinetic energy is freed instantaneously at movement start. The head will then rotate with a constant angular velocity, provided that viscous and other damping forces are negligible. On the other hand, with an actively contracting muscle, the prey reach time will be the shortest if the muscle contracts maximally throughout the movement. If we again neglect damping forces and assume that the contracting force does not depend strongly on contraction speed (e.g. through elastic elements in the muscle), then the head will continue to accelerate. These two cases, a given rate of kinetic energy (i.e. a constant acceleration) on the one hand, and a given amount of energy on the other hand (i.e. a constant angular velocity), will be considered in the model.

3.5. Model

We argued that the feeding mechanisms of *S. acus* and *C. scutatus* are extreme cases of pivot feeding, with regard to the length of their snouts. We hypothesize that this long snout is optimal for reaching the prey as fast as possible. In order to test this hypothesis and, additionally, to find the crucial parameters that determine the shape of the head and the snout, we developed a model. We compared the model predictions with anatomical measurements. Two factors are important for the model. We reasoned that a long snout would decrease the angle over which the head has to be rotated, decreasing the time to reach a prey at a given distance. On the other hand, lengthening of the snout increases the head's moment of inertia, increasing the time to reach the prey.

We put effort in keeping the model as simple and comprehensible as possible, without loosing predictive strength. We therefore leave out the R and r terms, which is as if the head turns about a stationary body. However, for the actual simulations, R and r were included. Other simplifications are discussed in appendix A, in footnote 2 and in the following text. In the general discussion, we will briefly address the influence of viscous damping as a result of drag. Behind each equation, we give the dimensions in square brackets, to facilitate reading.

Assume that the snout is an elliptic tube of length, height and width, lhw [m^3] and effective mass $m{=}1/4\alpha\rho\pi whl$ [kg] (see equation (2.1)). The moment of inertia of the snout is part of the total moment of inertia of the head,

$$\begin{aligned} J_{\text{total}} &= J_{\text{head}} + J_{\text{snout}} \\ &= J_{\text{head}} + \alpha\rho\pi whl\left(\frac{l^2}{3}+\frac{h^2}{4}\right) \\ &= J_{\text{head}} + \alpha\rho\pi\left(\frac{whl^3}{3}+\frac{wh^3l}{4}\right), \quad [\text{kg m}^2] \end{aligned} \tag{3.1}$$

We first consider the case of a given rate of kinetic energy, which amounts to a constant angular acceleration of the head. Let the head move with angular acceleration $\ddot{\theta}$, as a result of constant torque Q and moment of inertia J. Then, the lift angle will change as a function of time t,

$$\theta(t) = \frac{\ddot{\theta}}{2}t^2 = \frac{Q}{2J_{\text{total}}}t^2. \quad [\text{rad}]$$

The angle over which the head has to be rotated is $\theta_T{=}\arcsin(d/l)$, with prey distance d. Within the biological range of pipefishes, this lift angle is accurately approximated with $\theta_T{\approx}(d/l)$, so that the time to reach the prey is

$$T \approx \sqrt{\frac{2dJ_{\text{total}}}{lQ}}. \quad [\text{s}]$$

Filling in the moment of inertia (equation (3.1)), we get for the reach time

$$T \approx \sqrt{\frac{2\alpha\rho\pi d}{Q}\left(\frac{J_{\text{head}}}{\alpha\rho\pi l}+\frac{whl^2}{3}+\frac{wh^3}{4}\right)}. \quad [\text{s}] \tag{3.2}$$

One solution for this relation is shown in figure 4*a*. The right-hand side contains the sum of three factors: a hyperbola (c_1/l), a parabola (c_2l^2), and a constant. This relation has one minimum reach time, which corresponds to the optimal snout length. The optimal length is found by differentiating the equation with respect to snout length and finding the zero crossing

$$l_{\text{opt}}^3 = \frac{3J_{\text{head}}}{2\alpha\rho\pi wh}. \quad [\text{m}^3] \tag{3.3}$$

(We wrote the formula as l^3, to facilitate the comparison with equation (3.5).)

The model thus predicts that the optimal snout length is proportional with the third power root of J_{head} and inversely proportional with the third power root of the snout's cross-sectional area (wh). The torque and the prey's distance are irrelevant for the optimal snout length.

For the second case we consider, the head and the snout receive a given amount of kinetic energy E. The prey will be reached fastest with a constant angular velocity, as in *C. scutatus* (see §§3.1 and 3.4). The kinetic energy gained is

$$E = \frac{J_{\text{total}}\dot{\theta}_T^2}{2}, \quad [\text{J}]$$

where $\dot{\theta}_T$ is the angular velocity reached with such a kinetic energy. Rewriting this equation gives

$$\dot{\theta}_T = \sqrt{\frac{2E}{J_{\text{total}}}}. \quad [\text{rad s}^{-1}]$$

The reach time is the angular distance divided by the angular velocity,

$$T = \frac{\theta_T}{\dot{\theta}_T} \approx \frac{d}{l}\sqrt{\frac{J_{\text{total}}}{2E}}. \quad [\text{s}]$$

Substituting the moment of inertia (equation (2.1)) gives an equation similar to equation (3.1),

$$T \approx \sqrt{\frac{\alpha\rho\pi d^2}{2E}\left(\frac{J_{\text{head}}}{\alpha\rho\pi l^2}+\frac{whl}{3}+\frac{wh^3}{4l}\right)}. \quad [\text{s}] \tag{3.4}$$

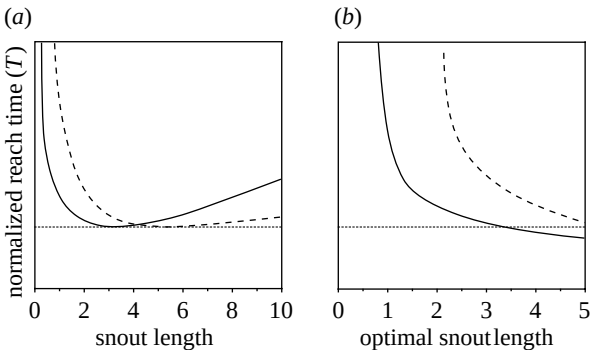

Figure 4. (*a*) Predicted time to reach the prey, T, as a function of dimensionless snout length. T was normalized with respect to the optimum in (*a*). Continuous curve: constant angular acceleration, equation (2.1). Dashed curve: fixed kinetic energy, equation (3.4). (*b*) Time to reach the prey as a function of optimal dimensionless snout length (equations (3.3) and (3.5)). For these parameters, equation (3.5) predicts that the dimensionless optimal length is at least 2.1 (dashed curve). Curves were calculated for dimensionless snout diameter $\sqrt{wh}\,J^{-1/5} = 0.2$ and snout diameter ratio $h/w{=}2.5$. In both (*a*) and (*b*) reach time T was normalized with respect to the minimal reach time in (*a*).

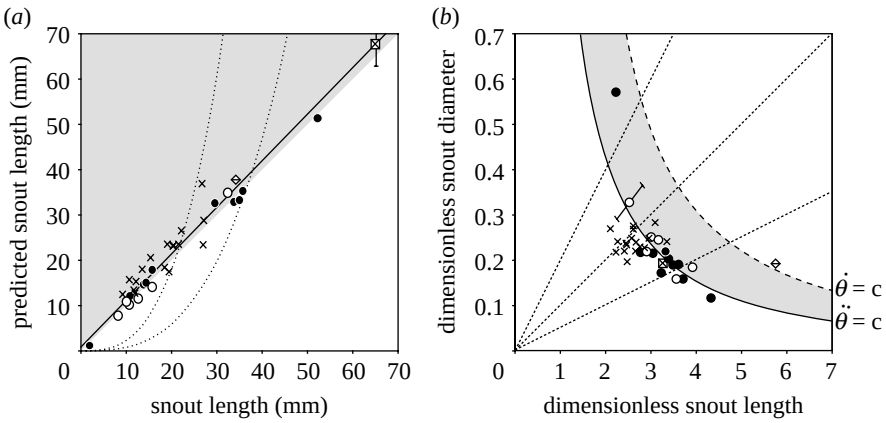

Figure 5. (*a*) Predicted and measured length of the snout for the species of appendix B. Crosses: *Hippocampus*; filled dots: *Syngnathus*; the juvenile *S. acus* has the smallest absolute snout length (*a*) and the largest dimensionless diameter (*b*). Open circles: other *Syngnathidae*; crossed diamond: *C. scutatus*; crossed square: *M. scolopax*. Regression line: predicted = 0.91 + 1.03 measured; $R^2 = 0.92$. Dotted curves: relationship predicted for isometric growth (predicted = $c \times$ measured$^{3/2}$). Grey region: snout is shorter than optimal. An estimated 95% confidence interval is shown for *M. scolopax* (note that the horizontal bar falls within the symbol). (*b*) The predicted and measured relation between dimensionless snout length and dimensionless cross-section (equation (3.3), continuous and equation (3.5), dashed). Grey area: the region predicted for intermediate velocity profiles. The dotted lines represent isometric scaling (length/diameter = constant). Error bar: the main source of uncertainty is J_{head}. Therefore, errors of dimensionless diameter and length strongly correlate and the largest error is in the direction of the error bar.

A typical solution for this equation is shown in figure 4. The solution for the optimal snout length is similar to equation (3.3),

$$l_{\mathrm{opt}}^3 - \frac{3}{4}h^2 l_{\mathrm{opt}} = 6\frac{J_{\mathrm{head}}}{\alpha\rho\pi wh}. \quad [\mathrm{m}^3] \qquad (3.5)$$

In order to keep the equations simple, we assumed that the acceleration phase is infinitely short. A finite acceleration phase will increase the reach time, but not the optimal snout length. We show this in appendix A.

3.6. Model results

In both modelled cases (equations (3.3) and (3.5)), the optimal snout length depended only on the snout's cross-sectional area and on the head's moment of inertia. This is shown in figure 4*a*: a short snout is relatively slow because it has to be rotated over a large angle, a very long one is relatively slow because it has a large moment of inertia.

To catch smaller prey, a narrower snout will be sufficient. Therefore, limiting the size of prey will lead to a longer optimal snout. But why should any species limit itself in the size of prey it can swallow? At first sight this appears evolutionarily non-adaptable because a narrow snout reduces the range of potential prey. The answer is given in figure 4*b*. Increasing the optimal snout length by reducing only the snout diameter (while keeping all other parameters constant) will strongly reduce the reach time, so that faster prey can be caught. This is exactly what can be expected for a species that optimizes its snout length to reach prey as fast as possible.

We then asked whether the model makes quantitative predictions, despite the simplifications. Using equation (3.5) for *C. scutatus* and equation (3.3) for the *Syngnathidae* and *M. scolopax*, we predicted the optimal snout lengths. These were close to the measured snout lengths (figure 5*a*). The species shown in figure 5*a* differ widely in size. This means that the relation could in part reflect a scaling effect. This scaling problem can be circumvented using dimensionless lengths.[4] The measured snout length and snout diameters become dimensionless, when divided by $\sqrt[5]{J_{\mathrm{head}}/\alpha\rho\pi}$.

The predicted relations between the dimensionless snout length and dimensionless snout diameter (equations (3.3) and (3.5)) are shown in figure 5*b*. The model predicts *C. scutatus* to lie on the upper curve and all other species on the lower one. Most species scatter around the lower curve. The measurements of *C. scutatus* and of the juvenile *S. acus* are on the curve for constant angular velocity. In the other species, apart from *Hippocampus*, the dimensionless snout diameter decreased with dimensionless snout length as predicted by the model. For *Hippocampus*, these two parameters were unrelated.

4. DISCUSSION

In the present study, we addressed the question why pipefishes have a long snout, and tested our idea that a long snout is an adaptation to capture prey as fast as possible. For this, we made a detailed analysis of the feeding kinematics and dynamics of two species. We analysed the mechanism from a functional viewpoint. We found that the mechanisms of *S. acus* and *C. scutatus* are very different, as discussed above (§3.4). That both nevertheless developed a long thin snout is additional evidence that a general principle is the cause. We developed the model for two ideal cases: for a constant rate of kinetic energy and for a given total amount of kinetic energy to reach the prey. We

[4]Choosing the scaling parameter for getting dimensionless measures is not trivial and can easily lead to contradictory results. We selected a scaling factor that is directly related to the head. The advantage of the moment of inertia over for example the volume is that it strongly reduces equations (3.2) and (3.4).

showed that both cases predict an optimal length for the snout. We further showed that a long, but narrow snout can be an evolutionary advantage, because it reduces the time needed to reach a prey. Indeed, pipefishes with a long snout tend to feed on faster, more mobile prey than shorter snouted species (Kendrick & Hyndes 2005).

Although the model contains important simplifications (we neglected viscous damping) and the moment of inertia of the head is difficult to estimate accurately, we applied the model to syngnathiform fishes with a large range of snout lengths. The model accurately predicted the absolute as well as the dimensionless snout lengths, on the basis of only the head's moment of inertia, the snout's cross-section and the velocity profile. We will first discuss the consequences of some simplifications and assumptions. We will then consider the influence of the velocity profile on the model predictions. Finally, we will discuss the validity of our theory for other predators.

Firstly, we estimated the centre of rotation of the head from the measurements of two species. This estimate may have caused errors in other species, especially in *Hippocampus*, because in these species the head makes a large angle with the body. Another important source of variable errors in the preserved specimen is the width of the head and the snout, because these are laterally non-rigid.

Secondly, we did not take into account the pressure inside the buccal cavity. However, a sub-ambient pressure is usually found as long as the opercular valves are closed (Muller & Osse 1984; Van Leeuwen 1984; Van Wassenbergh *et al.* 2005). Such a buccal sub-ambient pressure exerts a moment on the neck joint, and will therefore reduce the acceleration. As a result, such sub-ambient pressure is equivalent to an increased J_{head}. A buccal sub-ambient pressure therefore leads to an even longer predicted optimal snout.

Thirdly, the water surrounding the head and the snout damps the feeding movements due to viscous drag. The adult *S. acus* had a snout length of 35 mm, $h=3$ mm and $h/w=2.5$. It reaches a velocity of approximately $70\,\mathrm{rad\,s^{-1}}$, so that the Reynold's number is of the order of 10^4. This is in the intermediate range, between laminar and turbulent flows, where the drag coefficients are notoriously difficult to estimate. In the light of the high accelerations and increases in kinetic energy, viscous drag forces are probably relatively small in comparison with the inertial forces. However, especially in the small specimen, in which the Reynolds number is even smaller, they may be important. Drag depends on movement velocity and may therefore be more important on the snout than on the head. Loss of kinetic energy via the snout will most probably lead to an overestimation of the optimal length of the snout. This indeed seems to be the case in the juvenile *S. acus* (upper filled dot in figure 5*b*).

Fourthly, if the snout is short in comparison with the prey distance, the model predictions give systematic errors because the approximation $\theta_T \approx d/l$ is not applicable (until approx. 30°, $\sin(x)\approx x$). If the lift angle is relatively large, $\theta_T < d/l$, so that the optimal snout length will be underestimated. As in pipefishes, the lift angles are usually not very large, and the error does not affect the model results (we checked this by making the simulations without the simplification; figures 4 and 5).

Figures 4*b* and 5*b* show the influence of the velocity profile. Although the profiles of *S. acus* and *C. scutatus* were best approximated with a constant angular acceleration and a constant angular velocity, respectively, this is only an approximation.

How important were these possible error sources for our simulated data set? Different types of systematic and variable errors in the predicted data are possible (figure 5), and this gives some information about the most important error sources. Firstly, there can be evolutionary reasons for the snout not to be of optimal length for fast reaching, such as limitations by stiffness, mechanical strength and suction intensity. However, it appears very unlikely that a snout would be longer than optimal. This means that all points outside the grey area in figure 5*a* and to the right of the continuous curve (the dashed curve for *C. scutatus*) are on the 'unsafe' side. There does not seem to be a trend in the direction of the error, so most of the variability is probably due to the measurement errors and errors in the estimated centre of rotation.

An interesting difference between *Centriscidae* and *Syngnathidae* can be observed. During the rapid capture movement, the snout of *S. acus* is adducted (figure 2*h*), but that of *C. scutatus* is not. This means that *Centriscidae* must accelerate the water inside the snout to turn the head, but *Syngnathidae* not. If *Centriscidae* would feed on larger prey, the diameter of the rigid tube, the snout's cross-section should increase. For *Syngnathidae* only, the height, but not the width of the empty snout must increase (within certain constructional limits). This difference could have selected *Centriscidae* to feed on very small prey, and thus to have an even longer snout than *Syngnathidae* (figure 5*b*).

Is a rapid movement, driven by active muscle contraction feasible? White swimming muscle in *Myoxocephalus scorpius* can give a maximum power output of approximately $200\,\mathrm{W\,kg^{-1}}$ muscle at 12°C (James & Johnston 1998). Power depends on the torque (Q), lift angle (θ) and the reach time, T,

$$P = Q\theta/T = J\ddot{\theta}\theta/T. \quad [\mathrm{W} = \mathrm{J\,s^{-1}}],$$

For *S. acus* (the first specimen of appendix B), we estimated the moment of inertia J_{total} to be 23×10^{-9} kg m^2. For an acceleration of $23\,\mathrm{rad\,s^{-2}}$, a lift angle of $22\pi/180$ rad in 7×10^{-3} s, the power is 28×10^{-3} W. Even if we assume a power output of $100\,\mathrm{W\,kg^{-1}}$, the required power could be produced by $28\times10^{-3}/100=0.28$ g muscle tissue. This estimate appears to be feasible for the approximately 5 g epaxial musculature of a *S. acus* specimen of approximately 30 cm length.

The last issue we want to discuss is the possible relevance of our theory for other animals than pipefishes. Our model predicts that a thin snout should ideally be long enough to reach a prey in the

shortest time. Conversely, it also predicts that predators of large prey, which therefore need a wide mouth, optimally have short 'snouts'. As examples we already mentioned *P. flesus* and *C. sloani*. Whereas *P. flesus* has a moderately wide mouth and a slightly elongated head, *C. sloani* has an enormous mouth and a very short head. In our view, these predators are on the other side of the range of 'pipette feeders' than are the *Syngnathidae*. Thus, 'pipette feeding' seems to be not the most suitable name for catching prey by means of a rapid head turn. Instead, 'pivot feeding' describes the act better.

Another group of fishes where it would be interesting to apply the model are the catfishes (*Siluriformes*). Species of silurids can be found with a spectrum of snout lengths from very short to elongated Van Wassenbergh *et al.* (2006). Judging from the large angles over which they may turn the head to catch a prey, these movements presumably contribute significantly to catching the prey.

Moving away from suction feeders, there are many animals that do not suck their prey but nevertheless snap their prey by a rapid head turn. Examples are animals that typically turn the head sideways rather than upward, catching a prey between their long jaws. Examples are *Lepisosteus* (Lauder 1980), *Belone* (Porter & Motta 2004), crocodilians and a number of birds that can catch their prey with a rapid sideways swing of their long beaks. These animals have different head shapes than pipefishes, so that our model's predictions do not apply directly to these species. However, in most cases, adapting the model for such different shapes should be straightforward. It would be interesting to know whether indeed such widely differing species have snouts, beaks and bills of optimal length.

We thank the Museum Naturalis, Leiden (NL) for providing the preserved fishes. Maaike Schaffers, Coen van den Berg, Jurriaan de Groot, Hans Ovelgönne, Jasper Mortier, Erno Ruchtie and Andre Witkam have provided a rich source of ideas and measurements. We thank Arie Terlouw for his technical skills to perform several experiments and measurements. We are very grateful for the detailed comments and suggestions by the referees who saved us from many mistakes and unclarities. Finally, MdL wants to thank many friends for their enthusiasm and support.

APPENDIX A. THE ACCELERATION PROFILE

In the derivation of equation (3.4), we assumed that the acceleration was infinitely short. In this appendix we show that this assumption is justified, because the duration and profile of the acceleration phase affect the duration of the prey capture, but not the optimal snout length.

Tendons have an almost linear force–length relationship. This means that the torque, $Q(\theta)$, generated by the epaxial tendon will drop to zero with an increasing neck angle, $\theta(t)$, if the epaxial muscle does not compensate for this with a shortening contraction. We assume that the torque decreases linearly and becomes zero at time T_e

$$Q(\theta) = Q_0 - \frac{Q_0}{\theta_e}\theta \quad (\theta \le \theta_e), \quad [\mathrm{kg\,m^2 rad\,s^{-2}}] \quad (\mathrm{A}\ 1a)$$

$$Q(\theta) = 0 \quad (\theta > \theta_e), \quad [\mathrm{kg\,m^2\,rad\,s^{-2}}] \quad (\mathrm{A}\ 1b)$$

with initial torque Q_0, and zero torque at angle θ_e (with subscripts 0 and e for the start and end of the acceleration by stored elastic energy). We need to know the time to reach the prey $T = T_e + T_c$ (with subscript c for the constant angular velocity phase) at the final angle $\theta_T = \theta_e + \theta_c$. If we normalize $\hat{\theta}_e = \theta_e/\theta_T$ (the fraction of the lift movement where the torque is not zero), then

$$\theta_e = \hat{\theta}_e \theta_T, \quad [\mathrm{rad}] \quad (\mathrm{A}\ 2a)$$

$$\theta_c = (1 - \hat{\theta}_e)\theta_T. \quad [\mathrm{rad}] \quad (\mathrm{A}\ 2b)$$

The solution for equation (A 1*a*), when the torque is non-zero is

$$\theta(t) = \theta_e - \theta_e \cos\left(\frac{\pi}{2}\frac{t}{T_e}\right), \quad [\mathrm{rad}] \quad (\mathrm{A}\ 3a)$$

$$\dot{\theta}(t) = \theta_e \frac{\pi}{2T_e} \sin\left(\frac{\pi}{2}\frac{t}{T_e}\right), \quad [\mathrm{rad\,s^{-1}}] \quad (\mathrm{A}\ 3b)$$

$$\ddot{\theta}(t) = \theta_e \frac{\pi^2}{4T_e^2} \cos\left(\frac{\pi}{2}\frac{t}{T_e}\right), \quad [\mathrm{rad\,s^{-2}}] \quad (\mathrm{A}\ 3c)$$

so that time T_e, is found by substituting equations (A 2*a*) and (A 3*c*) for time $t = 0$

$$T_e^2 = \frac{\pi^2}{4}\frac{\theta_e}{\ddot{\theta}_0} = \frac{\pi^2}{4}\frac{\hat{\theta}_e \theta_T}{\ddot{\theta}_0}. \quad [\mathrm{s^2}]$$

To get the duration of the constant velocity phase, T_c, we first substitute equation (A 2*a*) into (A 3*b*) for time $t = T_e$

$$\dot{\theta}_c = \theta_e \frac{\pi}{2T_e} = \hat{\theta}_e \theta_T \frac{\pi}{2T_e}. \quad [\mathrm{rad\,s^{-1}}] \quad (\mathrm{A}\ 4)$$

The duration of the constant velocity phase, T_c, follows from equations (A 2*b*) and (A 4)

$$T_c = \frac{\theta_c}{\dot{\theta}_c} = \frac{\pi}{2}\frac{1 - \hat{\theta}_e}{\hat{\theta}_e}\sqrt{\frac{\hat{\theta}_e \theta_T}{\ddot{\theta}_0}}. \quad [\mathrm{s}]$$

so that the sum of T_e and T_c becomes

$$T = T_e + T_c = \frac{\pi}{2}\sqrt{\frac{\theta_T}{\hat{\theta}_e \ddot{\theta}_0}}. \quad [s]$$

Notice that θ_T is proportional to the snout length, whereas θ_e is independent of the snout's length, which implies that their ratio $\hat{\theta}_e$ is inversely proportional with the snout's length. This means that (analogously to the substitutions that led to equation (3.4))

$$T = \frac{\pi}{2}\sqrt{\frac{d^2}{\theta_e}\frac{J}{l^2 Q_0}}$$

$$= \sqrt{\frac{\pi^2}{4}\frac{\alpha\rho\pi d^2}{Q_0}\left(\frac{J_\mathrm{head}}{\alpha\rho\pi l^2} + \frac{whl}{3} + \frac{wh^3}{4l}\right)}, \quad [s] \quad (\mathrm{A}\ 5)$$

which differs from equation (3.4) by a constant factor and therefore predicts a longer reach time, but the same optimal snout length (equation (3.5)), irrespective of the duration of the acceleration phase.

APPENDIX B. LIST OF SPECIES

species	l (mm)	l (dimensionless)
Hippocampus abdominalis	27.1	0.195
Hippocampus comes	18.8	0.247
Hippocampus erectus	27.4	0.267
Hippocampus guttulatus	12.0	0.238
	12.5	0.232
	13.8	0.219
	19.4	0.236
	19.7	0.239
	20.6	0.223
	20.8	0.247
	21.9	0.226
	22.4	0.218
Hippocampus hippocampus	9.5	0.240
	12.2	0.274
	15.7	0.267
Hippocampus kuda	27.3	0.282
Hippocampus mohnikei	11.0	0.216
Syngnathus abaster	10.9	0.223
	13.9	0.159
	14.5	0.216
	15.8	0.173
Syngnathus acus (juvenile)	1.9	0.572
Syngnathus acus	33.9	0.204
	35.1	0.191
	35.8	0.190
	55.8	0.220
Hippichthys cyanospilus	12.7	0.246
Hippichthys penicillus	15.8	0.185
Nerophis lumbriciformis	8.3	0.329
Nerophis maculatus	10.2	0.220
	10.8	0.252
Syngnathoides biaculeatus	32.5	0.159
unknown (see caption)	27.7	0.117
Centriscus scutatus	31.4	0.157
Macrorhamphosus scolopax	65.1	0.194

List of the measured specimens, which all belong to the family *Syngnathidae*, except *C. scutatus* (*Centriscidae*) and *M. scolopax* (*Macrorhamphosidae*). Most specimens were borrowed from the collection of the Museum Naturalis, Leiden (NL), some of which were old (dating back to the nineteenth century). Where possible, we followed the scientific nomenclature from www.fishbase.org. The 'unknown' specimen was filed as *Siphostoma californiense* in the collection, which is not listed in fishbase.org, but could possibly be *Syngnathus californiensis*. Specimens of the same species are ordered by snout length (l). Snout length and dimensionless snout length are as given in figure 5*a*,*b*. Further information can be found in the electronic supplementary material.

APPENDIX C. LIST OF VARIABLES AND CONSTANTS

c, c_1, c_2	constants
d	initial distance between prey and snout (m)
h	dorso-ventral height of the snout (m)
H	dorso-ventral height of the head (m)
E	elastic or kinematic energy (J)
J	moment of inertia, with subscripts total, head and snout for the parts (kg m^2)
l	length of the snout from the neck joint (m)
L	length of the head (from the neck joint until where the mesethmoid and parasphenoid meet) (m)
m	mass (kg)
Q	torque exerted by the epaxial neck muscles (kg m^2 rad s^{-2})
r	distance between centre of rotation and snout centre of mass (m)
R	distance between centre of rotation and head centre of mass (m)
R^2	regression coefficient
T	time to reach the prey (s)
T_c	duration of constant velocity phase (appendix A) (s)
T_e	duration of acceleration phase (appendix A) (s)
t	time (s)
w	the snout's smallest width (m)
W	the head width (m)
α	added mass factor (1 + added mass) (dimensionless)
ρ	tissue density (kg m^{-3})
$\theta, \dot{\theta}, \ddot{\theta}$	rotation angle (rad), angular velocity (rad s^{-1}) and -acceleration (rad s^{-2})
$\ddot{\theta}_0$	initial angular acceleration (rad s^{-2})
θ_c	rotation during the constant angular velocity phase (rad)
θ_e	rotation during the angular acceleration phase (rad)

REFERENCES

Aerts, P. 1991 Hyoid morphology and movements relative to abductive forces during feeding in *Astatotilapia elegans* (*Teleostei*: *Cichlidae*). *J. Morphol.* **208**, 323–345. (doi:10.1002/jmor.1052080308)

Alexander, R. N. 1967*a* *Functional design in fishes*. London, UK: Hutchinson University Library.

Alexander, R. N. 1967*b* The functions and mechanisms of protrusible upper jaws of some acanthopterygian fish. *J. Zool. Lond.* **151**, 43–64.

Alexander, R. N. 1969 Mechanisms of the feeding action of a cyprinid fish. *J. Zool. Lond.* **159**, 1–15.

Alexander, R. N. 1970 Mechanisms of the feeding action of various teleost fishes. *J. Zool. Lond.* **162**, 145–156.

Altermatt, R. U. 1991 *Zur Kopfanatomie des Schnepfenfisches* Macrorhamphosus scolopax (*Linnaeus, 1758*) (*Teleostei, Syngnathiformes*). Ph.D. thesis, Universität-Basel.

Anker, G. C. 1989 Morphology of the joints and ligaments in the head of a generalized *Haplochromis* species: *Haplochromis elegans* Trawas 1933 (*Teleostei*, *Cichlidae*). III. The hyoid and the branchiostegal apparatus, the

branchial apparatus and the shoulder girdle apparatus. *Neth. J. Zool.* **39**, 1–40.

Bergert, B. A. & Wainwright, P. C. 1997 Morphology and kinematics of prey capture in the syngnathid fishes *Hippocampus erectus* and *Syngnathus floridae*. *Mar. Biol.* **127**, 563–570. (doi:10.1007/s002270050046)

Branch, G. M. 1966 Contributions to the functional morphology of fishes: part III: the feeding mechanism of *Syngnathus acus* L. *Zoologica Africana* **2**, 69–89.

Daniel, T. L. 1984 Unsteady aspects of aquatic locomotion. *Am. Zool.* **24**, 121–134.

Deban, S. M. & Olson, W. M. 2002 Biomechanics: suction feeding by a tiny predatory tadpole. *Nature* **420**, 41–42. (doi:10.1038/420041a)

Drost, M. R. & van den Boogaart, J. G. M. 1986 A simple method for measuring the changing volume of small biological objects, illustrated by studies of suction feeding by fish larvae and of shrinkage due to histological fixation. *J. Zool. Lond.* **209**, 239–249.

James, R. S. & Johnston, I. A. 1998 Scaling of muscle performance during escape responses in the fish *Myoxocephalus scorpius* L. *J. Exp. Biol.* **201**, 913–923.

Jungersen, H. F. E. 1908 Ichthyotomical contributions, I. The structure of the genera *Amphisile* and *Centriscus*. *Dansk. Vidensk. Naturv.* **6**, 41–109.

Jungersen, H. F. E. 1910 Ichthyotomical contributions, II. The structure of the *Aulostomidae*, *Syngnathidae* and *Solenostomidae*. *Dansk. Vidensk. Naturv.* **8**, 269–363.

Kayser, H. 1961 Vergleichende Untersuchung über Vorstreckmechanismen der Oberkiefer bei Fischen. Der Bau und die Funktion des Kiefer- und Kiemenapparates von Knochenfischen der Gattungen *Ammodytes* und *Callionymus*. *Zool. Beitr.* **7**, 321–446.

Kendrick, A. J. & Hyndes, G. A. 2005 Variations in the dietary compositions of morphologically diverse syngnathid fishes. *Environ. Biol. Fishes* **72**, 415–427. (doi:10.1007/s10641-004-2597-y)

Kuiter, R. H. 2000 *Seahorses, pipefishes and their relatives—a comprehensive guide to Syngnathiformes*. Cranswick, UK: TMC Publishing.

Lauder, G. V. 1980 Evolution of the feeding mechanism in primitive actinopterygian fishes: a functional anatomical analysis of *Polypterus*, *Lepisosteus*, and *Amia*. *J. Morphol.* **163**, 283–317. (doi:10.1002/jmor.1051630305)

Motta, P. J. 1984 Mechanics and functions of jaw protrusion in teleost fishes: a review. *Copeia* **1**, 1–18. (doi:10.2307/1445030)

Muller, M. 1987 Optimization principles applied to the mechanism of neurocranium levation and mouth bottom depression in bony fishes (*Halecostomi*). *J. Theor. Biol.* **126**, 343–368. (doi:10.1016/S0022-5193(87)80241-2)

Muller, M. 1996 A novel classification of planar four-bar linkages and its application to the mechanical analysis of animal systems. *Phil. Trans. R. Soc. B* **351**, 689–720. (doi:10.1098/rstb.1996.0065)

Muller, M. & Osse, J. W. M. 1984 Hydrodynamics of suction feeding in fish. *Trans. Zool. Soc. Lond.* **37**, 51–135.

Nelson, J. S. 1984 *Fishes of the world*, 2nd edn. London, UK: Wiley Interscience Publication.

Nelson, J. S. 2006 *Fishes of the world*, 4th edn. London, UK: Wiley.

Osse, J. W. M. 1969 Functional morphology of the head of the perch (*Perca fluviatilis* L): an electromyographic study. *Neth. J. Zool.* **19**, 289–392.

Osse, J. W. M. 1985 Jaw protrusion, an optimization of the feeding apparatus of teleosts? *Acta Biotheoretica* **34**, 219–232. (doi:10.1007/BF00046786)

Porter, H. T. & Motta, P. J. 2004 A comparison of strike and prey capture kinematics of three species of piscivorous fishes: Florida gar (*Lepisosteus platyrhincus*), redfin needlefish (*Strongylura notata*), and great barracuda (*Sphyraena barracuda*). *Mar. Biol.* **145**, 989–1000. (doi:10.1007/s00227-004-1380-0)

Tchernavin, V. V. 1953 *Feeding mechanisms of a deep sea fish Chauliodus sloani* Schneider. London, UK: The Trustees of the British Museum.

Van Leeuwen, J. L. 1984 A quantitative study of flow in prey capture by rainbow trout, *Salmo gairdneri* with general consideration of the actinopterygian feeding mechanism. *Trans. Zool. Soc. Lond.* **337**, 171–227.

Van Leeuwen, J. L. & Muller, M. 1984 Optimum sucking techniques for predatory fish. *Trans. Zool. Soc. Lond.* **37**, 137–169.

Van Wassenbergh, S., Aerts, P. & Herrel, A. 2005 Scaling of suction feeding kinematics and dynamics in the african catfish, *Clarias gariepinus*. *J. Exp. Biol.* **208**, 2103–2114. (doi:10.1242/jeb.01682)

Van Wassenbergh, S., Aerts, P. & Herrel, A. 2006 Hydrodynamic modeling of aquatic suction performance and intra-oral pressures: limitations for comparative studies. *J. R. Soc. Interface* **3**, 507–514. (doi:10.1098/rsif.2005.0110)